Characterization of buried cylinders and spheres by pulsed infrared thermography

Florencio Garrido and Agustín Salazar[a]
Departamento de Física Aplicada I, Escuela Técnica Superior de Ingeniería de Bilbao, Universidad del País Vasco, Alameda Urquijo s/n, 48013 Bilbao, Spain

Fernando Alonso and Idurre Sáez-Ocáriz
Centro de Tecnologías Aeronáuticas (CTA), Parque Tecnológico de Álava, Juan de la Cierva 1, 01510 Miñano, Spain

A theoretical model to calculate the time evolution of the surface temperature of an opaque sample containing buried cylinders or spheres, after the absorption of a short light pulse, has been developed. To do this we first calculate the temperature of the material when it is illuminated by a modulated light beam. Then, based on the analogy between the Helmholtz equation and the Laplace transform of the heat diffusion equation we obtain the Laplace transform of the solution. Finally, using the inverse Laplace transform we find the time evolution of the surface temperature heated by a short light pulse. Measurements performed by an infrared camera on a calibrated sample confirm the validity of the model. © *2005 American Institute of Physics*. [DOI: 10.1063/1.2132097]

I. INTRODUCTION

Active infrared thermography has been used for the thermal characterization and nondestructive evaluation of a wide variety of materials.[1] In this nondestructive testing technique some energy is given to the specimen to be inspected in order to obtain significant temperature differences at the sample surface, in the presence of subsurface anomalies. Various methods have been developed according to the way the sample is heated. One of the most popular is pulsed thermography, where the sample is heated briefly by a light pulse and the subsequent surface temperature evolution is recorded as a function of time by means of an infrared camera. By solving the heat diffusion equation with the appropriate boundary conditions the surface temperature of a material containing one-dimensional buried defects (multilayered systems, delaminations, cracks, etc.) has been calculated.[2] Then, inversion procedures have been developed to determine depth, thickness, and thermal properties of the defects.

In this work we calculate the temperature evolution of an opaque material containing parallel buried cylinders or spheres after being heated by a short light pulse. Recently, the frequency-dependent temperature $T(\mathbf{r},\omega)$ of such a material when heated by a modulated light beam of frequency $f(\omega=2\pi f)$ has been published.[3,4] The method used is based on the multiple scattering of the thermal waves, that are generated at the sample surface, by the subsurface structures. Here we present a model to convert the modulated solutions $T(\mathbf{r},\omega)$ into pulsed solutions $T(\mathbf{r},t)$. Based on the analogy between the Helmholtz equation and the Laplace transform of the heat diffusion equation we obtain the Laplace transform of the solution. Then, using the inverse Laplace transform we find the time evolution of the surface temperature heated by a short light pulse. Measurements performed by an

infrared camera on a calibrated sample with a subsurface cylinder made of different materials (air, water, and steel) confirm the validity of the model. This work confirms the ability of pulsed thermography as a quantitative method to study fiber-reinforced composites as well as particulate-reinforced composites.

II. THEORY

In this section we first calculate the surface temperature of an opaque material with subsurface cylinders or spheres when its surface is illuminated by a periodic light beam. Then, starting from these modulated solutions we calculate the surface temperature evolution after being heated by a short duration light pulse.

A. Buried cylinders

Let us consider an infinite cylinder of radius a, whose center is buried at a depth d beneath the surface of an opaque and semi-infinite material that is illuminated by a modulated light beam of intensity I_0 and frequency $f(\omega=2\pi f)$. The geometry of the problem is shown in Fig. 1(a). We take into consideration the lack of adherence between cylinder and matrix by introducing a thermal contact resistance R_{th} between them. In the following indices M and C stand for
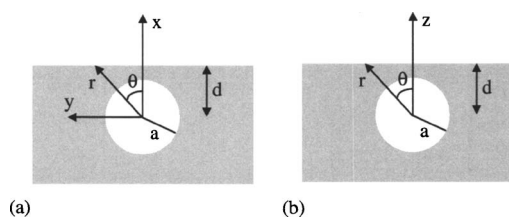
FIG. 1. Geometry of a semi-infinite material containing a buried cylinder (a) or sphere (b).

matrix and cylinder, respectively. Assuming that heat losses are negligible, the surface temperature can be written as[3]

$$T(r,\theta,\omega) = \frac{I_0(1-R)i}{2K_M q_M} e^{iq_M(d-r\cos\theta)}$$
$$+ 2\sum_{m=-\infty}^{\infty} A_m H_m(q_M r) e^{im\theta}, \qquad (1)$$

where $q=\sqrt{i\omega/D}$ is the thermal wave vector, R is the optical reflection coefficient of the surface, D is the thermal diffusivity, K is the thermal conductivity, and H_m is the mth order of the Hankel functions of the first kind. The first term in Eq. (1) represents the incident plane thermal wave starting at the sample surface, while the second one accounts for the scattered waves coming out from the cylinder. Equation (1) requires the knowledge of the $2m+1$ constants $A_m(m=-\infty,\infty)$ that can be obtained from the $2m+1$ equations given by the boundary conditions at the cylinder surface (existence of a thermal resistance and heat flux continuity):[3]

$$A_m\frac{1-Y_m^C/Z_m^C}{S_m^M-Z_m^M Y_m^C/Z_m^C} + \sum_{n=-\infty}^{\infty} A_n H_{m+n}(2q_M d)$$
$$= -\frac{I_0(1-R)i}{2K_M q_M} e^{iq_M d} i^{-m}, \qquad (2)$$

where

$$S_m^M = \frac{J_m(q_M a)}{H_m(q_M a)}, \quad Z_m^M = \frac{J_m'(q_M a)}{H_m'(q_M a)},$$

$$Y_m^C = \frac{J_m(q_C a) + K_C R_{\text{th}} J_m'(q_C a)}{H_m(q_M a)}, \text{ and } Z_m^C = \frac{K_C}{K_M}\frac{J_m'(q_C a)}{H_m'(q_M a)}, \qquad (3)$$

being

$$J_m'(qa) = \left.\frac{dJ_m(qr)}{dr}\right|_{r=a} \text{ and } H_m'(qa) = \left.\frac{dH_m(qr)}{dr}\right|_{r=a}$$

the derivatives of the Bessel and Hankel functions, respectively.

Similar expressions have been found for the surface temperature of an opaque plate containing an unlimited number of parallel cylinders of different radii buried at different depths.[3]

B. Buried spheres

Now we consider a sphere of radius a buried at a depth d beneath the surface, under the same material and heat transport conditions as in Sec. II A. The geometry of the problem is shown in Fig. 1(b). Index S stands for the sphere. The surface temperature can be written as[4]

$$T(r,\theta,\omega) = \frac{I_0(1-R)i}{2K_M q_M} e^{iq_M(d-r\cos\theta)}$$
$$+ 2\sum_{m=0}^{\infty} B_m h_m(q_M r) P_m(\cos\theta), \qquad (4)$$

where h_m is the mth order of the spherical Hankel functions of the first kind and P_m is the Legendre functions. The second term in Eq. (4) represents the scattered waves coming out from the sphere. Equation (4) requires the knowledge of the $m+1$ constants $B_m(m=0,\infty)$ that can be obtained from the $m+1$ equations given by the boundary conditions at the sphere surface (existence of a thermal resistance and heat flux continuity):[4]

$$B_m\frac{1-Y_m^S/Z_m^S}{S_m^M-Z_m^M Y_m^S/Z_m^S} + \sum_{n=0}^{\infty} (-1)^n B_n Q_{0,m,0n}(2d)$$
$$= -\frac{I_0(1-R)i}{2K_M q_M} e^{iq_M d}(1+2m) i^{-m}, \qquad (5)$$

where

$$S_m^M = \frac{j_m(q_M a)}{h_m(q_M a)}, \quad Z_m^M = \frac{j_m'(q_M a)}{h_m'(q_M a)},$$

$$Y_m^S = \frac{j_m(q_S a) + K_S R_{\text{th}} j_m'(q_S a)}{h_m(q_M a)},$$

and

$$Z_m^S = \frac{K_S}{K_M}\frac{j_m'(q_S a)}{h_m'(q_M a)}, \qquad (6)$$

being

$$j_m'(qa) = \left.\frac{dj_m(qr)}{dr}\right|_{r=a} \text{ and } h_m'(qa) = \left.\frac{dh_m(qr)}{dr}\right|_{r=a}$$

the derivatives of the spherical Bessel and Hankel functions, respectively.

Generalization to the case of a set of buried spheres can be found in Ref. 4.

C. From modulated to pulsed illumination

The solutions in the frequency domain $T(\mathbf{r},\omega)$ can be smoothly converted into solutions of the Laplace domain $\bar{T}(\mathbf{r},p)$ by replacing $i\omega$ by $-p$, and $I_0/2$ by $\bar{P}(p)$, the Laplace transform of the power distribution of the light pulse. For instance, in the case of a Dirac pulse whose power distribution writes $P(t)=Q_0\delta(t)$ its Laplace transform is $\bar{P}(p)=Q_0$, where Q_0 is the energy per unit area delivered by the pulse. In the case of an exponential power distribution of the type $P(t)=Q_0(t/\tau^2)\exp[-(t/\tau)]$, that represents properly the shape of a laser pulse, the Laplace transform is $\bar{P}(p)=Q_0/(1+p\tau)^2$.[5]

Then, using the inverse Laplace transform the time-dependent solution $T(\mathbf{r},t)$ is obtained. To do this we use the Stehfest algorithm,[6] a numerical method that provides an approximate value of the required solution:
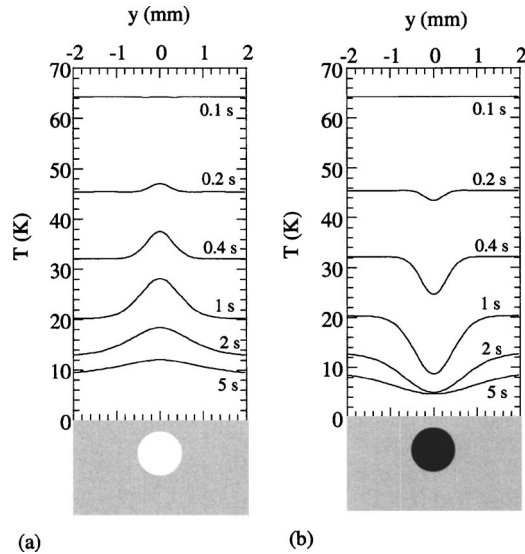
FIG. 2. Theoretical lateral scans of the surface temperature of an epoxy matrix containing a cylinder of radius $a=0.5$ mm buried at a depth $d-a=0.3$ mm. (a) Air cylinder and (b) graphite cylinder.

$$T(\mathbf{r},t) \approx \frac{\ln(2)}{t}\sum_{j=1}^{N} V_j \bar{T}\left[\mathbf{r}, j\frac{\ln(2)}{t}\right], \qquad (7)$$

where the quantity $j\ln(2)/t$ substitutes for the Laplace variable p. The coefficients V_j are given by

$$V_j = (-1)^{N/2+j}\sum_{k=[(j+1)/2]}^{Min(j,N/2)} \frac{k^{N/2}(2k)!}{(N/2-k)!(k-1)!(j-k)!(2k-j)!}, \qquad (8)$$

where N is even and k is computed using integer arithmetic. For "smooth" $\bar{T}(\mathbf{r},p)$ functions the Stehfest algorithm gives very accurate results.[7] In principle, the larger the value of N, the more accurate the numerically inverted solution. However, N is limited by truncation errors. A characteristic of the V_j coefficients is that their absolute values tend to increase as N does. Thus, the use of large N values causes subtraction of one large number from another, with resulting loss of accuracy. Computation with various values of N is used to check whether the same result is obtained. In our calculations N values between 10 and 18 give good convergence, provided high-precision arithmetic is used.

III. NUMERICAL CALCULATIONS

We have calculated the time evolution of the surface temperature above room temperature of an epoxy matrix ($K_M=0.10$ W m^{-1} K^{-1}, $D_M=0.13$ mm^2 s^{-1}, and $Q=10^4$ J/m^2) containing a subsurface cylinder of radius $a=0.5$ mm buried at a depth $d-a=0.3$ mm, after receiving a Dirac pulse. Lateral scans at different times after the heating pulse are shown in Fig. 2. Two cases are considered: a thermal isolating cylinder (air: $K_C=0.026$ W m^{-1} K^{-1} and $D_C=22$ mm^2 s^{-1}) and a good thermal conducting cylinder (graphite: $K_C=150$ W m^{-1} K^{-1} and $D_C=95$ mm^2 s^{-1}). As can be seen the presence of the isolating (good conducting) cylinder produces an increase (decrease) of the temperature
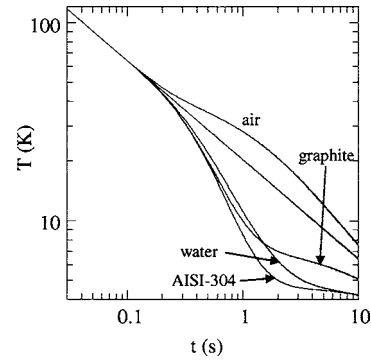
FIG. 3. Calculations of the surface temperature decay after the heating pulse just over the center of a buried cylinder of radius $a=0.5$ mm buried at a depth $d-a=0.3$ mm in an epoxy matrix. Cylinders made of four different materials are considered. The straight line corresponds to a point far away from the cylinder.

above the cylinder with respect to the regions that are free of buried cylinders. This is explained by the fact that heat accumulates above the air cylinder, while the graphite cylinder acts as a heat sink. On the other hand, for short times after the Dirac pulse, the propagating heat has not reached the buried cylinder and therefore the surface temperature is flat. Then as the time goes by the thermal contrast between the region above the cylinder and the region far from it increases, until it reaches a maximum, that for these thermal and geometrical parameters is about 1 s after the heating pulse. At the same time, heat propagates laterally and the temperature rise affects regions that are far from the buried cylinder.

The time evolution of the surface temperature just over the center of the buried cylinder is shown in a logarithmic scale in Fig. 3. The same matrix and the same geometry as before are used. Four cylinders are considered in order to study the influence of the material they are made of. Air, water ($K_C=0.60$ W m^{-1} K^{-1} and $D_C=0.144$ mm^2 s^{-1}), graphite, and AISI-304 stainless steel ($K_C=14.0$ W m^{-1} K^{-1} and $D_C=4.0$ mm^2 s^{-1}). The straight line, whose slope is -0.5, represents the temperature history of a point that is not affected by the subsurface cylinder. With respect to this reference line worse thermal conductors such as air produce a temperature rise, while better thermal conductors such as graphite, steel, or even water produce a temperature decrease. Note that the thermal contrast is higher for steel than for graphite, although this last one is a better thermal conductor. Both are much better thermal conductors than the epoxy matrix. In such a case, it has been demonstrated that K and D are degenerate and only their ratio K/D, the heat capacity of the cylinder, influences the surface temperature.[8] As this ratio is higher for steel than for graphite the first one produces a higher thermal contrast.

The influence of the cylinder radius is analyzed in Fig. 4. Air cylinders of various radii buried at a constant depth $d-a=0.3$ mm in the same epoxy matrix as before are considered. As can be seen, the time at which the temperature separates from the straight line of slope -0.5, that corresponds to the absence of subsurface cylinder, is governed by the depth $d-a$, while the cylinder radius a controls the shape of the curve. As the cylinder radius goes to infinity the result con-
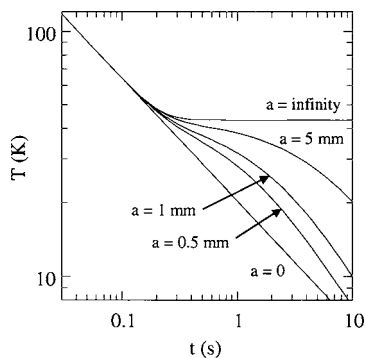
FIG. 4. Calculations of the surface temperature decay just over the center of a buried air cylinder in an epoxy matrix. The depth $d-a=0.3$ mm is kept fixed while varying the radius.

FIG. 5. Calculations of the surface temperature decay just over the center of a buried graphite cylinder of radius $a=0.5$ mm buried at a depth $d-a$ $=0.3$ mm in an epoxy matrix. Various thermal resistances are considered. The straight line corresponds to a point far away from the cylinder.

verges to a horizontal straight line, that is, the expected behavior corresponding to a plate that is 0.3 mm thick.[2]

Finally, the influence of the thermal resistance between cylinder and matrix is analyzed in Fig. 5. Calculations are performed for the same matrix as before with a subsurface cylinder of graphite of radius $a=0.5$ mm buried at a depth $d-a=0.3$ mm. As can be seen, thermal resistances lower than 10^{-4} m^2 K W^{-1} cannot be distinguished from the perfect thermal contact. As the thermal resistance increases the thermal contrast with respect to the straight line of slope -0.5 diminishes. For higher thermal resistances the thermal contrast is positive for short times but it becomes negative for longer times. This behavior can be explained as follows. A thermal resistance can be understood as a very thin air layer between matrix and inclusion. For short times after the heating pulse the propagating heat reaches this air layer and therefore a temperature rise is produced. As time is further increased the heat reaches the graphite that acts as a heat sink and consequently the temperature diminishes.

Calculations performed in the same epoxy matrix with a subsurface sphere show similar results as those presented for a subsurface cylinder, and therefore they are not shown here.

IV. EXPERIMENTAL RESULTS AND DISCUSSION

The validity of the theory has been tested experimentally by measuring the surface temperature of a calibrated sample that has been prepared by drilling a hole in a black epoxy matrix ($K_C=0.10$ W m^{-1} K^{-1}, $D_C=0.13$ mm^2 s^{-1}, and a $=2.5$ mm). The cylindrical hole is not completely parallel to the surface, in such a way that the depth on one side is d $-a=550$ μm and on the other side is $d-a=450$ μm. The

sample has been illuminated by two flash lamps (6 kJ each) and the surface temperature has been recorded by an infrared camera (Thermacam SC 2000 from FLIR systems, with a 320×240 pixel sensor) at a rate of 50 frames/s. Successive measurements have been performed with the cylindrical hole filled with air, distilled water, and two AISI-304 steel rods, whose diameters are 4.50 and 4.95 mm, that in the following will be referred as steel(a) and steel(b), respectively. When introducing a solid rod whose diameter is smaller than the diameter of the cylindrical hole, a thermal resistance appears between matrix and rod, whose value is defined as R_{th} $=e/K_{air}$, where e is the thickness of the air layer between matrix and rod. Therefore, in the case of a steel rod of 4.95 mm in diameter inside a cylindrical hole of 5 mm in diameter the equivalent thermal resistance is R_{th} $\approx 10^{-3}$ m^2 K/W, while for the rod of 4.50 mm in diameter the thermal resistance is $R_{th}\approx 10^{-2}$ m^2 K/W. It is worth noting that the thickness of the air layer is not uniform all around the circumference and therefore the above values should be considered as effective thermal resistances. On the other hand, as the surface temperature is more sensitive to the upper part of the cylinder we could conclude that only the thermal resistance at the top of the cylinder should be taken into account.

Temperature maps of the epoxy surface with the air cylinder at four different times after the heating pulse are shown in Fig. 6. To better visualize the effect of the buried cylinder on the surface temperature, we present the temperature contrast (ΔT), i.e., the temperature rise with respect to a region far from the cylinder. As expected, the air cylinder produces
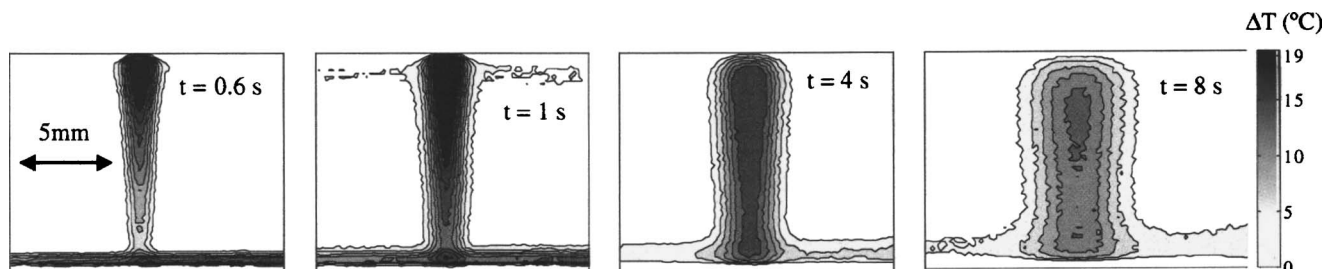
FIG. 6. Measurements of the temperature contrast (ΔT), normalized to the region without buried cylinder, for a black epoxy sample containing an air cylinder of radius $a=2.5$ mm buried at a depth $d-a=0.5$ mm. Four different times after the light pulse are shown.
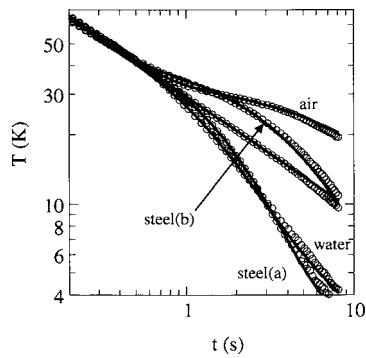
FIG. 7. Temperature decay after the flash light just above the center of a subsurface cylindrical hole of radius $a=2.5$ mm buried at a depth $d-a=0.5$ mm in a black epoxy matrix. The hole is filled with air, water, and two steel rods. The straight line corresponds to a point far away from the buried cylinder. Measurements (circles) and theory (continuous lines).

FIG. 8. Lateral scans of the surface temperature contrast 2 and 4 s after the light flash for the same conditions of Fig. 7. The experimental results are shown for the cylindrical hole filled with air (●), water (○), steel(a) (×), and steel(b) (+). Theory (continuous lines).

a temperature increase above the buried cylinder. On the other hand, the vertical temperature gradient above the cylinder that can be seen in each thermogram is a consequence of the lack of parallelism of the cylindrical hole with respect to the sample surface, indicating that the hole is closer to the surface at the top than at the bottom of the thermogram.

To obtain quantitative information we study the central region of the sample where the hole depth $d-a$ is about 0.5 mm. The time evolution of the surface temperature just above the center of the buried cylinder is shown in Fig. 7. Each experimental curve is the average of the temperature of 10 close pixels. The circles represent the experimental data while the continuous lines are the theoretical calculations using Eq. (1). For these calculations we have used the geometrical and thermal parameters given above. The agreement between the experimental data and theoretical curves is very good for the four cylinders, except for times longer than 5 s. In our opinion this is due to the influence of heat losses, mainly due to convection effects, that have not been taken into account in the model. The straight line with slope -0.5 (both circles and solid line) corresponds to a point far away from the cylinder. Here the influence of heat losses at large times can also be seen.

Lateral scans of the temperature contrast (ΔT), 2 and 4 s after the light flash, are shown in Fig. 8. The dots stand for air, circles for water, × for steel(a), and + for steel(b). The continuous lines are the theoretical calculations using Eq. (1). Again a very good agreement can be appreciated.

As a conclusion we can say that a general expression for the time-dependent temperature of an opaque sample with buried parallel cylinders or spheres after a flash pulse has
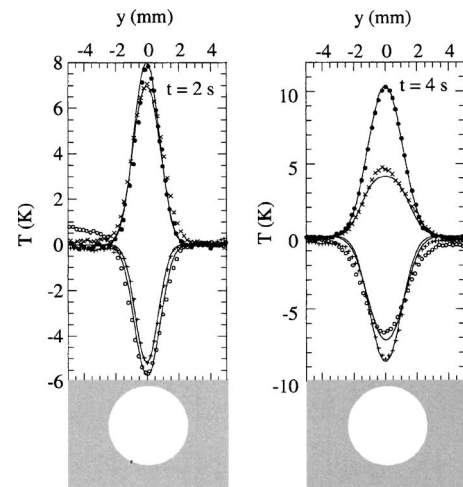
been presented. This model is interesting because it simulates the internal structure of fiber- and particulate-reinforced composites. Measurements of the temperature decay using an infrared camera on a black epoxy sample containing a subsurface cylinder filled with air, water, or steel confirm the validity of the model.

ACKNOWLEDGMENTS

[1]X. Maldague, *Theory and Practice of Infrared Technology for Nondestructive Testing* (Wiley, New York, 2001).
[2]X. Maldague, *Nondestructive Evaluation of Materials by Infrared Thermography* (Springer-Verlag, London, 1993).
[3]J. M. Terrón, A. Salazar, and A. Sánchez-Lavega, J. Appl. Phys. **91**, 1087 (2002).
[4]F. Garrido and A. Salazar, J. Appl. Phys. **95**, 140 (2004).
[5]Equations (1)–(6) are valid for harmonic solutions of the form $T(\mathbf{r},t) = T(\mathbf{r})e^{-i\omega t}$. If solutions with positive time exponential $[T(\mathbf{r},t)=T(\mathbf{r})e^{+i\omega t}]$ are used, then Eqs. (1)–(6) are still valid provided the wave vector q is changed by iq. In this case, the substitution to convert the modulated solution to the Laplace transform is $i\omega=p$.
[6]H. Stehfest, Commun. ACM **13**, 47 (1970).
[7]J. C. Krapez, J. Appl. Phys. **87**, 4514 (2000).
[8]A. Salazar, F. Garrido, A. Oleaga, and R. Celorrio, J. Appl. Phys. **98**, 013513 (2005).